Journal of Applied Polymer Science

Preparation and characterization of benzoxazine based nanocomposites: Comprehensive study in curing kinetics and enhanced thermal stabilities

Yue Lin,[1] Corinne A. Stone,[2] Steve J. Shaw,[2] Mo Song[1]
[1]Department of Materials, Loughborough University, Loughborough LE11 3TU, United Kingdom
[2]The Defence Science and Technology Laboratory, Porton Down, Salisbury SP4 0JQ, United Kingdom
Correspondence to: M. Song (E-mail: m.song@lboro.ac.uk)

ABSTRACT: Several bisphenol-A benzoxazine (BEN) based nanocomposites incorporated with several polyhedral oligomeric silsesquioxane (POSS), carbon nanotubes (CNTs), and clays, were prepared successfully. The influences of the nanofillers on curing kinetics, network formation, and thermal stability of the BEN were investigated comprehensively. The addition of the nanofillers showed different influence on curing kinetics of BEN. Furthermore, the incorporation of the nanofillers showed good improvement on thermal stability of BEN. An increase of 70 and 336°C at the onset and the half-life decomposition temperature were observed with the addition of 5 wt % 30B clay in nitrogen atmosphere. With the incorporation of 5 wt % POSS, the half-life of decomposition and char yield enhanced by 280°C and 13 wt % in nitrogen atmosphere. For the 4 wt % MWCNT-COOH/BEN nanocomposite, the half-life of decomposition and char yield at 800°C increased by 286°C and 14 wt % in nitrogen atmosphere, respectively. © 2015 Wiley Periodicals, Inc. J. Appl. Polym. Sci. **2015**, *132*, 41903.

KEYWORDS: composites; crosslinking; degradation; thermosets

Received 4 July 2014; accepted 14 December 2014
DOI: 10.1002/app.41903

INTRODUCTION

Recently, polybenzoxazines, a newly developed class of polymerised phenolic system, have received a wide range of interest, due to their good mechanical performance, molecular design flexibility, and thermal and flame retardant properties. More importantly, polybenzoxazines under spotlight is that it overcomes the problems of traditional novolac and resole phenolic systems, such as, poor shelf life.[1,2] The polybenzoxazine also performs several unique features, (a) near-zero shrinkage upon curing, (b) low water absorption, (c) T_g much higher than cure temperature for some polybenzoxazine based materials, (d) relatively good thermal stability, (e) no strong acid catalysts required for curing, and (f) release of no by-products during curing.[3] Although polybenzoxazines possess a lot of unique features, there are some shortcomings, for example, low processability, and high curing temperature. To overcome these shortages during applications, benzoxazine is usually mixed with other polymers and fillers to prepare polymer blends and composites. A variety of polymers, such as rubber,[4–7] polycarbonate,[8] poly (e-caprolactone) (PCL),[9,10] polyurethane (PU),[11,12] and epoxy,[13–16] have been used to improve processability of benzoxazine. Apart from polymer blends, the influence of the incorporation of nanofillers on properties of benzoxazine has been studied by a few groups.[17–31] Huang *et al.*[21] prepared polybenzoxazine/POSS nanocomposites through the reactions of a multifunctional vinyl-terminated benzoxazine-POSS with a benzoxazine monomer at various compositional ratios. The mobility of the benzoxazine network was significantly hindered by the incorporation of the silsesquioxane core units. Furthermore, the thermal stability and mechanical properties of the nanocomposites were gradually improved with the increasing POSS content. Agag and Takeichi[32] demonstrated the preparation of polybenzoxazine-clay nanocomposites by the *in situ* polymerization of allyl functionalized benzoxazine monomer, in the presence of two different types of organoclay. The glass transition temperature (T_g) of the nanocomposites decreased firstly, and then increased with the increasing organoclay content. These results implied a change of curing mechanism and network formation of the benzoxazine with the incorporation of organoclay. Furthermore, the thermal stability of the nanocomposites was better than that of the neat resin. Wang *et al.*[33] functionalized multi-walled carbon nanotubes (MWCNTs) using benzoxazine-containing compound (BPA-FBz) and polymer (PFBz) as modifiers through a Diels-Alder reaction. They then

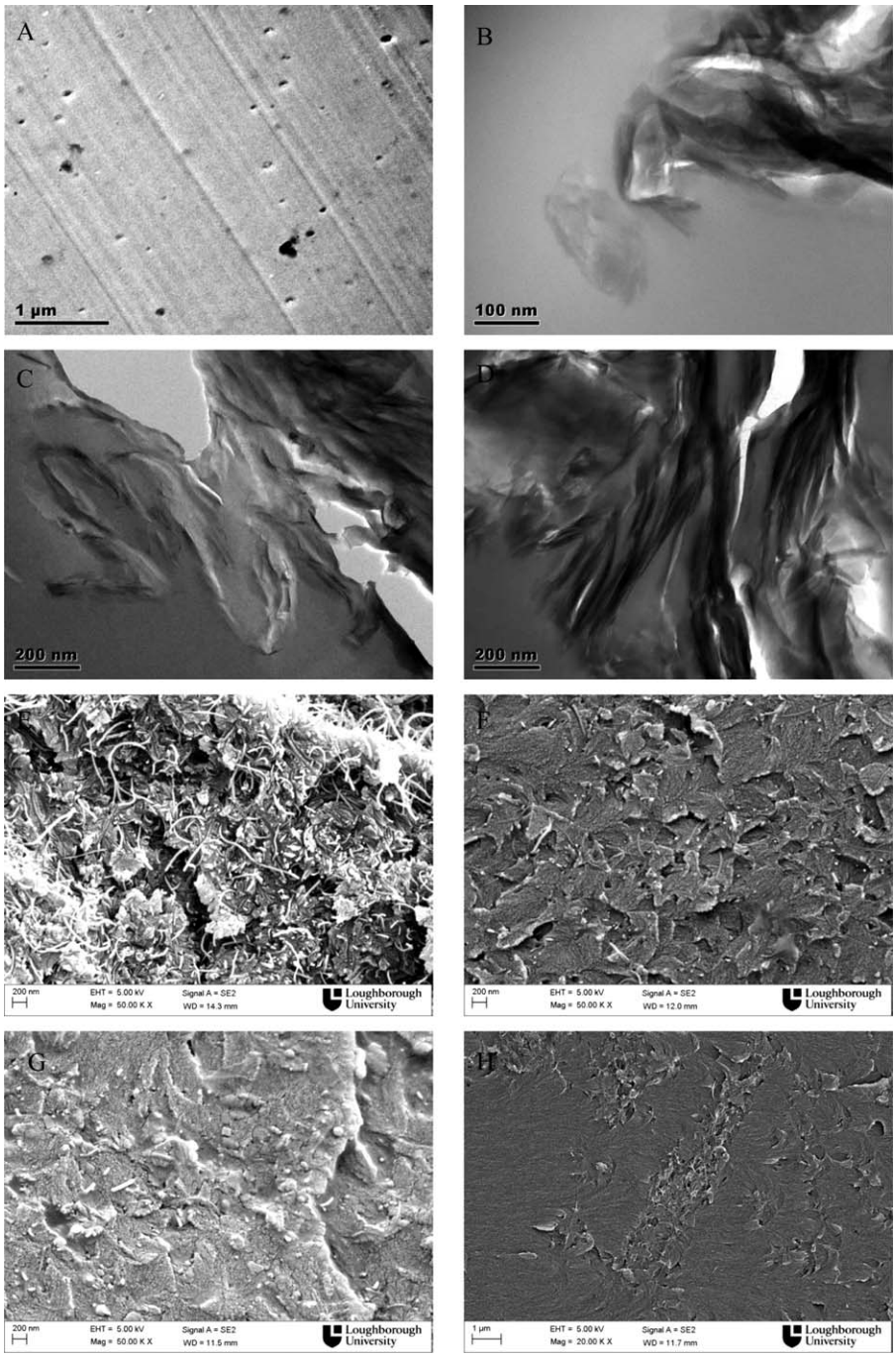

Figure 1. SEM (A, E, F, G, H) and TEM (B–D) images of the nanocomposites of the BEN incorporated with 5 wt % POSS (A), 5wt % Na^+/BEN (B), 1 wt % 30B/BEN (C), 1 wt % 20A/BEN (D), 2 wt % MWCNT/BEN (E), 2 wt % MWCNT-OH (F), 2 wt % MWCNT-COOH (G), and 2 wt % SWCNT-OH (H).

fabricated MWCNT-FBz and MWCNT-PFBz crosslinked nanomaterials by using press molding and other thermal-forming processes. The surface electrical conductivities and electrical conductivities of the crosslinked pellets of MWCNT-FBz and MWCNT-PFBz were measured as 0.05 S cm^{-1} and 7×10^{-5} S cm^{-1}. Alhassan *et al.*[34] prepared the graphene oxide/polybenzoxazine nanocomposites using a solvent casting method. The incorporation of graphene oxide led to a decrease in glass transition temperature of the matrix, which is due to the reactive nature of graphene oxide. Furthermore, graphene oxide was found to react with the benzoxazine to form a gel. It is believed that the attractive properties were attributed to the good compatibility between the polybenzoxazine matrix and MWCNT-FBz.

Although progress has been made, few groups have comprehensively focused on the curing kinetics and network formation of benzoxazine based nanocomposites. This is vitally interesting

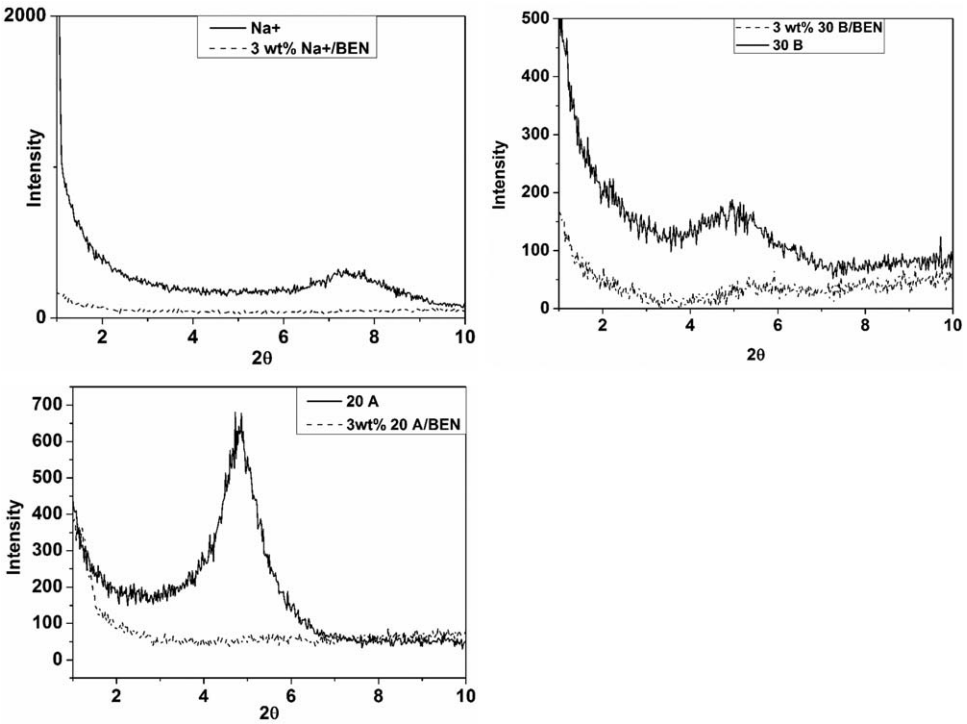

Figure 2. XRD patterns for Na^+ clay, 30B clay, 20A clay, and their BEN/clay nanocomposites.

and important, particularly for thermoset based nanocomposites. For example, the processing ability and properties of thermoset based nanocomposites depends on various factors, such as the composition of nanocomposites, dispersion of nanofillers, and influence of the nanofillers on the crosslinking reaction. To develop high performance benzoxazine based nanocomposites, a clear understanding of curing kinetics and network formation in the benzoxazine resin during cure is essential, so that the properties of the benzoxazine based nanocomposites can be subsequently designed or controlled. On the other hand, in order to meet the ever-increasing demand for benzoxazine with high thermal stability, it is very important to study the thermal decomposition of the benzoxazine and its nanocomposites. Thus, in this work, the curing kinetic and network formation of the benzoxazine incorporated with several nanofillers were studied. The influence of the nanofillers on the thermal stability of the benzoxazine was studied systematically as well.

EXPERIMENTAL

Materials

Araldite® MT 35600 CH Bisphenol-A Benzoxazine resin (BEN) was provided by Huntsman Ltd. TriSilanolPhenyl POSS (POSS-OH, $C_{42}H_{38}O_{12}Si_7$, $M_W = 931.34$ g/mol) and AminopropylIsobutyl POSS (POSS-NH_2, $_{31}H_{71}NSi_8O_{12}$, $M_W = 874.58$ g/mol) were purchased from Hybrid Plastics. The unmodified sodium clay (Cloisite® Na^+) and the organoclay (Cloisite® 20A and Cloisite® 30B) were purchased from Southern Clay Products. The modifier for Cloisite® 20A is dimethyl, dehydrogenated tallow, and quaternary ammonium (2M2HT). For Cloisite® 30B, it is methyl, tallow, bis-2-hydroxyethyl, quaternary ammonium (MT2EtOH). The pristine multiwalled carbon nanotube (MWCNT), functionalized multiwall carbon nanotubes (MWCNT-OH and MWCNT-COOH), and functionalized single-wall carbon nanotube (SWCNT-OH) were purchased from Chengdu Institute of Organic Chemistry, Chinese Academy of Science. The multiwall carbon nanotubes (MWCNTs) have a length of ~50 μm and a diameter of 8–15 nm. For the hydroxyl functionalized single-walled carbon nanotube used (SWCNT-OH), the length is between 5 and 30 μm, and the diameter is 1–2 nm. All the solvents used were purchased from Sigma-Aldrich, UK.

Preparation of BEN Mixtures Incorporated with the Nanofillers

All BEN mixtures incorporated with clays and POSS were prepared as follows. The BEN resin was firstly held at 100°C for

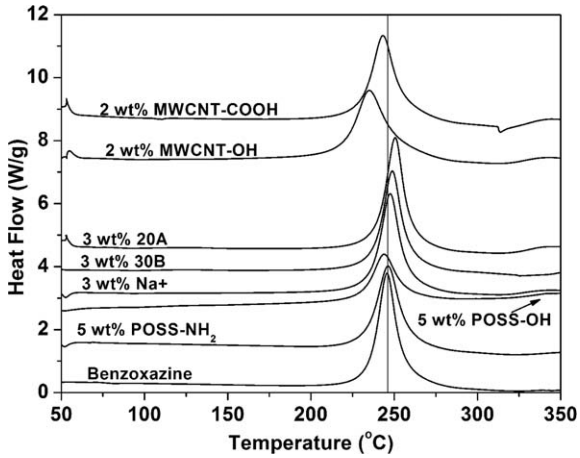

Figure 3. DSC plots of benzoxazine and its nanocomposites in nitrogen atmosphere (60 mL/min) with heating rate of 10°C/min.

Table I. Onset, Peak, and End Temperatures, and Enthalpy of the Nonisothermal Cure of the BEN with Different Nanofillers

Nanofillers	Onset temperature (°C)	Peak temperature (°C)	End temperature (°C)	Duration (min)	$\triangle H$ (J/g)
Neat BEN	210	246	288	7.8	354
5 wt % POSS-OH	206	244	284	7.8	173
5 wt % POSS-NH_2	209	246	291	8.2	304
3 wt % Na^+	207	248	292	8.5	325
3 wt % 30B	207	249	288	8.1	317
3 wt % 20A	209	251	290	8.1	345
2 wt % MWCNT-OH	185	219	294	10.9	351
2 wt % MWCNT-COOH	201	243	291	9.0	342

30 min with magnetic stirring to remove moisture. Next, the BEN was heated to 120°C, and calculated amounts of the nanofillers were added into the low viscosity resin to prepare the mixtures. These mixtures were stirred at 120°C for 120 min. After mixing, all the mixtures prepared were sealed in glass bottles and stored at −20°C for further use.

BEN/CNT mixtures were prepared by the following procedure. CNTs were first dispersed in acetone (1 mg/1 mL) with assistance of ultrasonication (300 W power, 30 min) at room temperature. The BEN was held at 100°C for 30 min in a vacuum oven to remove moisture, and then was dissolved in acetone. Following this, the BEN/acetone solution was mixed with

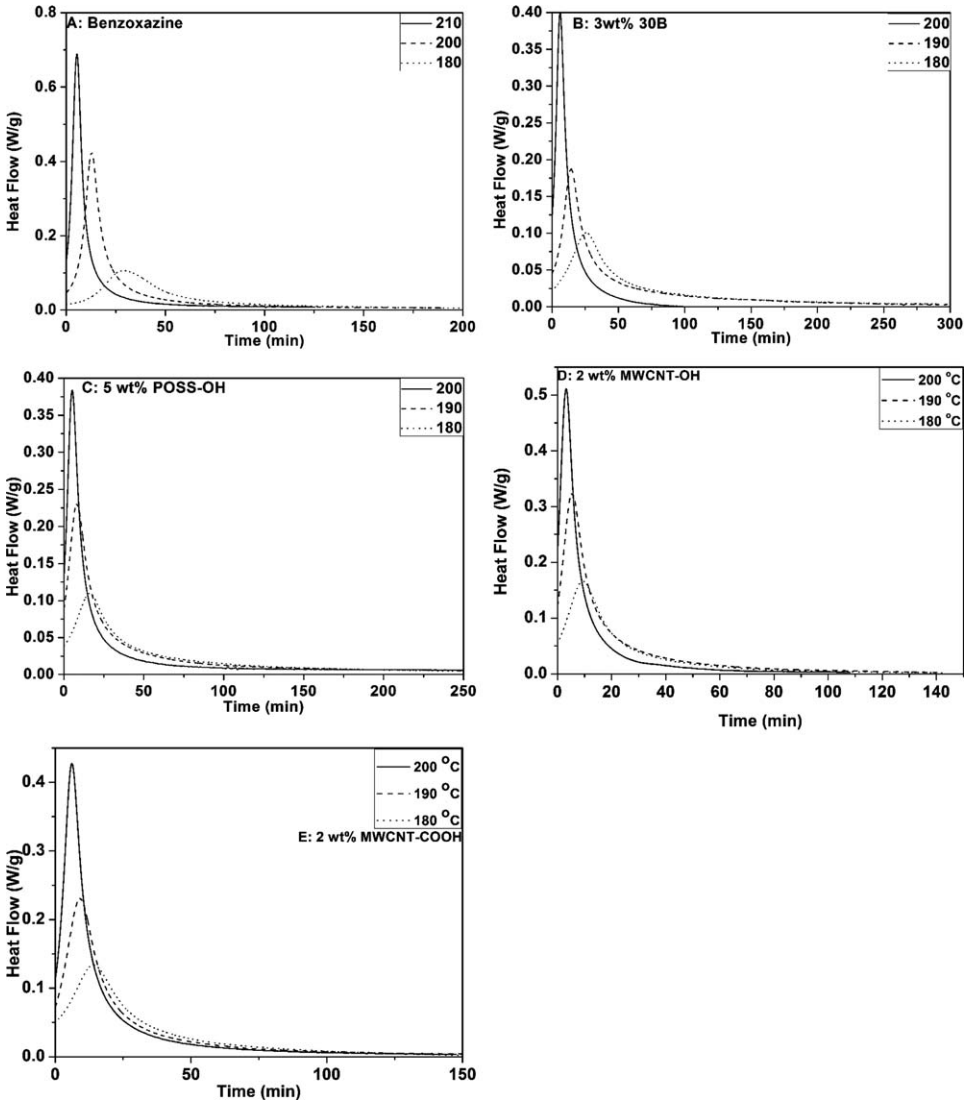

Figure 4. Plots of heat flow versus curing time for BEN/nanofiller systems at different curing temperatures.

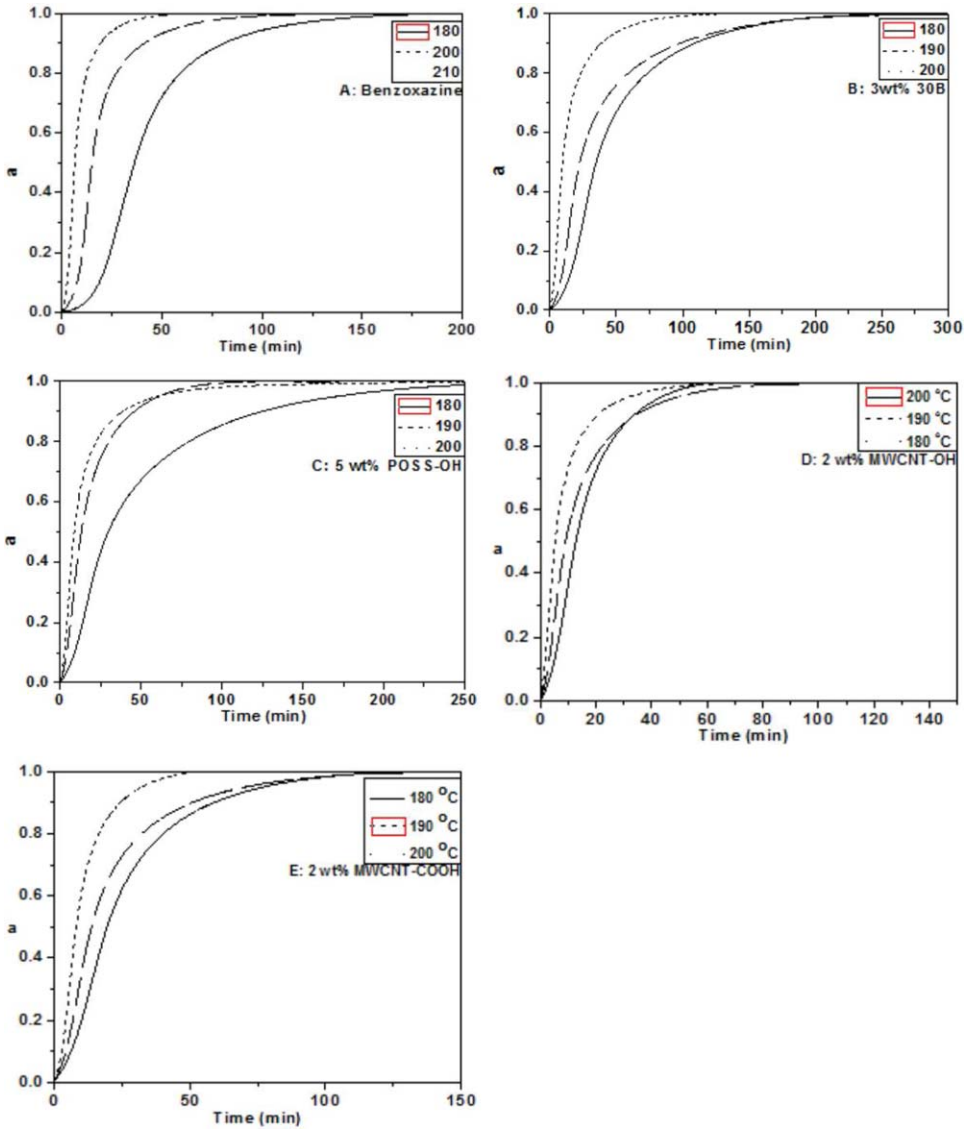

Figure 5. Plots of conversion rate (α) versus curing time for BEN/nanofiller systems at different curing temperatures. [Color figure can be viewed in the online issue, which is available at wileyonlinelibrary.com.]

theCNTs/acetone solution with magnetic stirring for 2 h. The solvent was then volatilized. The resultant was further dried in a vacuum oven at 80°C. The BEN/CNTs mixtures prepared were sealed in glass bottles and stored at −20°C for further use.

Preparation of BEN Based Nanocomposites

For all BEN based nanocomposites, the curing procedure is as follows. The BEN based mixtures were firstly precured at 100°C for 30 min, to make sure all the moisture was removed. Afterwards, the mixtures were cured at 200°C for 2 h, and followed by postcuring at 260°C for another 2 h.

Characterization

A TA Instruments DSC 2920 calorimeter was employed for differential scanning calorimetry (DSC) and modulated-temperature differential scanning calorimetry (MTDSC) measurements. Nitrogen was used as the purge gas (60 mL/min). All the dynamic experiments were carried out using DSC. Samples were heated from 50 to 350°C with a heating rate of 10°C/min. For all the quasi-isothermal experiments, MTDSC was employed. Samples were held at selected temperatures with a modulation amplitude of 0.5°C per 60 s. Fourier transform infrared (FTIR) spectra of the sample coated on KBr pellet were recorded from 4000 to 400 cm^{-1} using a Shimadzu FTIR-8400s spectrophotometer with a 4 cm^{-1} resolution over 128 scans. Raman spectra were recorded from 100 to 3500 cm^{-1}, on a Jobin Yvon Horiba high-resolution LabRam 800 Raman microscope system, which contains an optical microscope adapted to a double grating spectrograph and a CCD array detector. The laser excitation was provided by a Spectra-Physics model 127 helium–neon laser operating at 35 mW of 633 nm output. All the samples for FTIR and Raman experiments were cured in a DSC cell in N_2 atmosphere (60 mL/min). To determine whether the clays were fully exfoliated in the CY matrix, X-ray diffraction (XRD) patterns of the CY/clay nanocomposites were

Table II. Autocatalytic Model Constants for the BEN and Its Nanocomposites

Sample	Temperature (°C)	k_1 ($\times 10^4$ s^{-1})	k_2 ($\times 10^4$ s^{-1})	m	n	$\ln A_1$	$\ln A_2$	E_1 (kJ/mol)	E_2 (kJ/mol)
BEN	180	0.08	24.2	0.928	1.77	48	38	229	132
	200	0.979	154.6	1.469	2.629				
	210	3.57	192.1	1.3	2.2685				
3 wt % 30B	180	0.484	24.5	1.03	2.19				
	190	0.843	47.8	1.08	2.76	34	24	165	113
	200	3.11	87	1.07	2.42				
5 wt % POSS-OH	180	0.7276	18.7	0.79	2.33				
	190	2.22	40	0.876	2.01	28	29	142	132
	200	3.56	82.3	0.99	2.39				
2 wt % MWCNT-OH	180	2.23	36.1	0.86	1.549				
	190	3.09	55	0.83	2.088	18	17	100	84
	200	6.89	92.7	0.90	2.06				
2 wt % MWCNT-COOH	180	1.56	31.8	1.02	1.928				
	190	2.01	48.2	0.98	2.201	34	24	56	94
	200	2.93	91.9	1.06	2.036				

obtained by using a Philip-X9 Pert X-ray diffractometer (anode 40 kV, filament current 35 mA) with nickel-filtered CuKa ($\lambda = 0.1542$ nm) radiation at a scan speed of 1°/min. To observe the dispersion of the nanofillers in the CY matrix, scanning electron microscopy (SEM) images of the fracture surface of the CY/POSS nanocomposites were taken by field emission gun scanning electron microscopy (FEGSEM) (LEO 1530VP instrument). The samples were fractured at room temperature. The samples with fractured surface on the top were placed on specimen holder using double-sided carbon conductive tap. Gold coating was applied for better conductivity. Transmission electron microscopy (TEM) was employed to observe the state of the nanofillers in the CY matrix as well, using a JEOL 2100 FX instrument. The CY based nanocomposites were cut into the ultra-thin films using a microtome, and then were dropped on a copper grid for direct TEM imaging. Thermogravimertic analysis (TG) was performed on a DSC-TG 2950 instrument. The samples were heated from room temperature to 1000°C at a heating rate of 10°C/min. The rate of gas (air or nitrogen) was 60 mL/min.

RESULTS AND DISCUSSION

Dispersion of the Nanofillers in the BEN Based Nanocomposites

Figure 1 shows the TEM and SEM images of the cured BEN based nanocomposites. The POSS was dispersed well in the BEN matrix without obvious aggregation [Figure 1(A)]. As shown in Figure 1(B–D), the Na^+ clay, the 30B clay, and the 20A clay layers were exfoliated in the BEN matrix. Figure 1(E–H) shows SEM images of the various BEN/CNT nanocomposites (all at 2 wt %). All the functionalized MWCNTs were well dispersed at a nanoscale level in the BEN matrix, with no indication of aggregation taking place. However, for the pure MWCNT/BEN nanocomposite, and the SWCNT-OH/BEN nanocomposite, the CNT bundles were visible at the micro-scale.

Table III. The Kinetic Activation Energy and the Pre-exponential Factor for the BEN and Its Nanocomposites

Sample	α	0	0.1	0.2	0.3	0.4	0.5	0.6	0.7	0.8	0.9	1
BEN	E (kJ/mol)	229	87	96	104	110	116	120	124	127	130	133
	ln$A$	49	15	18	21	22	24	25	27	28	28	29
3 wt % 30B	E (kJ/mol)	165	119	115	114	113	113	114	114	114	114	114
	ln$A$	34	23	23	23	23	23	24	24	24	24	24
5 wt % POSS-OH	E (kJ/mol)	142	103	109	114	118	121	124	127	129	131	132
	ln$A$	28	20	22	23	24	25	26	27	28	28	29
2 wt % MWCNT-OH	E (kJ/mol)	100	84	83	83	83	84	84	84	84	85	85
	ln$A$	18	15	15	16	16	16	16	16	17	17	17
2 wt % MWCNT-COOH	E (kJ/mol)	56	78	84	86	88	90	90	91	92	92	93
	ln$A$	6	13	15	16	17	17	18	18	18	19	19

Table IV. Analytical Results of the FTIR Spectra of the Pure BEN Resin Cured at 180°C

Wave number (cm^{-1})	Assignment	Bond
1230	Asymmetric C—O stretching	Cyclic ether C—O—C
1173	C—O stretching	Phenol C—OH
3520	O—H stretching	Phenol C—OH
1493	C=C stretching	trisubstituted benzene ring [9]
1483	C=C stretching	tetrasubstituted benzene ring
1600	Oxazine ring C—N—O stretching	N—C—O
1573	C—N stretching	C—N—C
1620	Aromatic C=O stretching	Aromatic C=O
934	Oxazine ring stretching[39]	Oxazine ring
858	N—H wagging and weisting	N—H

To further examine the state of clay layers for the different clays in the BEN matrix, the d-spacing of Na^+ clay, 30B clay, 20A clay, 3 wt % BEN/Na^+ nanocomposite and 3 wt % BEN/30B nanocomposite, and 3 wt % BEN/20A nanocomposite were measured using XRD and the results are shown in Figure 2. The original d-spacing of the clays for Na^+, 30B, and 20A were 1.17, 1.85, and 2.42 nm, respectively.[35] For all the nanocomposites, it was noted that there was no peak in the range of 1° to 10°. This result indicated the exfoliation of the clays in the BEN matrix.

Curing Kinetic of Benzoxazine and Its Nanocomposites

Figure 3 shows DSC plots of BEN and its nanocomposites in nitrogen atmosphere. Table I lists the parameters obtained from DSC experiments. It is clearly that the addition of POSS did not show any catalytic effect. For the clay/BEN nanocomposites, the incorporation of the clays delayed the curing reaction, indicating as the increase of peak temperature by up to 5°C. It is interested that the incorporation of MWCNTs showed good catalytic effect. For 2 wt % MWCNT-OH, the peak temperature decreased by 27°C. Furthermore, the reaction enthalpy of 5 wt % POSS-OH/BEN system was 173 J/g, significantly lower than that of pure BEN which is 354 J/g. This observation indicates that the incorporation of POSS-OH hindered the network formation of the BEN. The better catalytic effect of CNTs than that of clays and POSS may be due to the higher concentration of functional group and larger specific surface area.

To further examine the influence of the nanofillers on the curing kinetics of the BEN, the activation energies of the BEN and its nanocomposites during the cure were calculated based on an empirical rate equation proposed by Kamal.[35–38]

Figure 4 shows the plots of heat flow versus curing time for BEN/nanofiller systems at different curing temperatures. Figure 5 shows the plots of conversion rate (α) versus curing time for BEN/nanofiller systems at different curing temperatures. It is clearly shown that the reaction was accelerated by increasing the temperature. Table II summarizes the kinetic parameters calculated from the isothermal MDSC experiments using Kamal's equation, for the BEN and its nanocomposites. It is clearly shown that the increasing temperature accelerates the reaction.

Table III shows the kinetic activation energy and the pre-exponential factor for the BEN and its nanocomposites. Table IV shows the analytical results of the FTIR spectra of the pure BEN resin cured at 180°C. Figure 6 shows the kinetic activation energy versus conversion for the BEN and its nanocomposites. With the incorporation of the POSS-OH, the activation energy is lower than that of the pure BEN at the very beginning of the cure. However, with the proceeding of the cure, the activation energy increased and exceeded that of pure BEN after conversion of 0.1. This observation implies that the incorporation of POSS-OH hindered the network formation of the BEN, which is accordance with the dynamic DSC result. With the incorporation of the 30B clay, the activation energy is lower than that of the pure BEN at the very beginning and after middle of the cure process, but became higher at the conversion of 0.1–0.4. Thus, considering over all cure process, there is no obvious acceleration effect shown. On the other hand, the incorporation of the functionalized MWCNTs displayed good acceleration effects, the activation energy dropped dramatically at the very beginning, and was lower than that of neat BEN throughout the whole curing process. It should be noticed that MWCNT-OH showed better acceleration effects than that of MWCNT-COOH due to the lower activation energy across

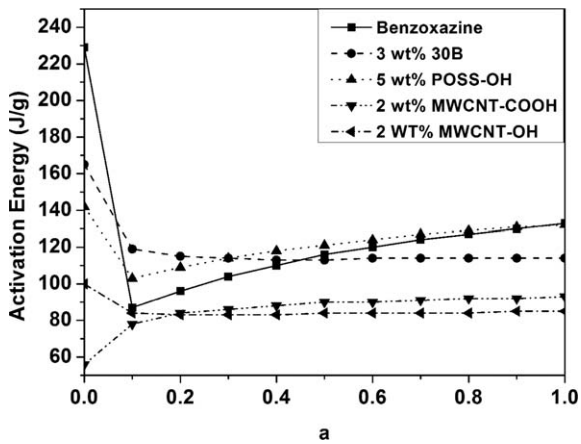

Figure 6. Kinetic activation energy versus conversion for the BEN and its nanocomposites.

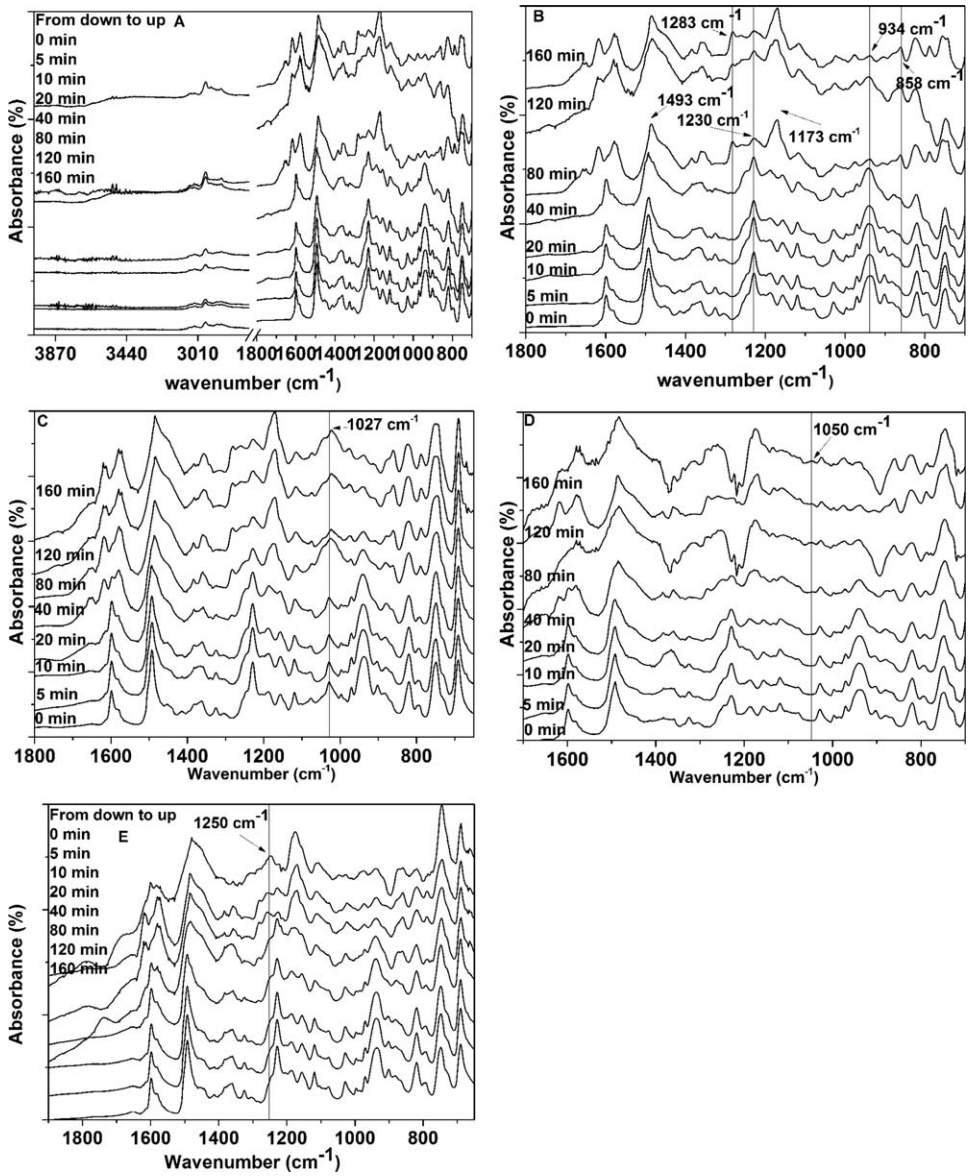

Figure 7. FTIR spectra for the pure BEN and its nanocomposites cured at 180°C in nitrogen atmosphere (60 mL/min). (A) original, (B) enlarged A, (C) 3 wt % 30B/BEN, (D) 5 wt % POSS-OH/BEN, (E) 2 wt % MWCNT-COOH. For clarification, the spectra were shift parallel, and were calibrated basing the absorption band of phenyl ring symmetric breathing vibration near 1500 cm^{-1}.

most of the curing process of the BEN. The results are accordance with the dynamic DSC result.

Network Formation of Benzoxazine and Its Nanocomposites

Figure 7(A,B) shows the FTIR spectra for the pure BEN resin cured at 180°C in nitrogen atmosphere (60 mL/min). The characteristic absorption bands of the BEN structure were observed at 1600, 1493, 1230, and 934 cm^{-1}, due to stretching of C—N—O group in oxazine ring, stretching of C=C bond in benzene ring, the asymmetric stretching of cyclic C—O—C ether group in oxazine ring, and the stretching of oxazine ring itself, respectively. The cure of the BEN resin can be followed by monitoring the corresponding absence in the absorbance bands of oxazine ring at 1600, 1230, and 934 cm^{-1}. With increased curing time, the absorbance bands of oxazine ring disappeared because of the open of the ring. Another new band at 858 cm^{-1} assigning to N—H wagging and twisting, indicated the occurrence of the ring opening as well. The characteristic band of trisubstituted benzene ring at 1493 cm^{-1} shifted to 1573 cm^{-1}, which indicated the tetrasubstitution of the benzene ring. Furthermore, a new band at 1173 cm^{-1} assigned to C—O stretching of phenol groups, indicated the formation of the phenol structure. The presence of absorbance bands at 1573 and 1620 cm^{-1} indicating the C—N stretching and aromatic C=O stretching, also provided evidence of the oxazine ring opening and cure. It should be noticed here that the intensity of the absorbance bands of oxazine ring remained the same until 40 min, and then the absorbance bands suddenly disappeared or decreased. Furthermore, the intensity of the new bands changed little with the curing time. This observation reflects the fact that

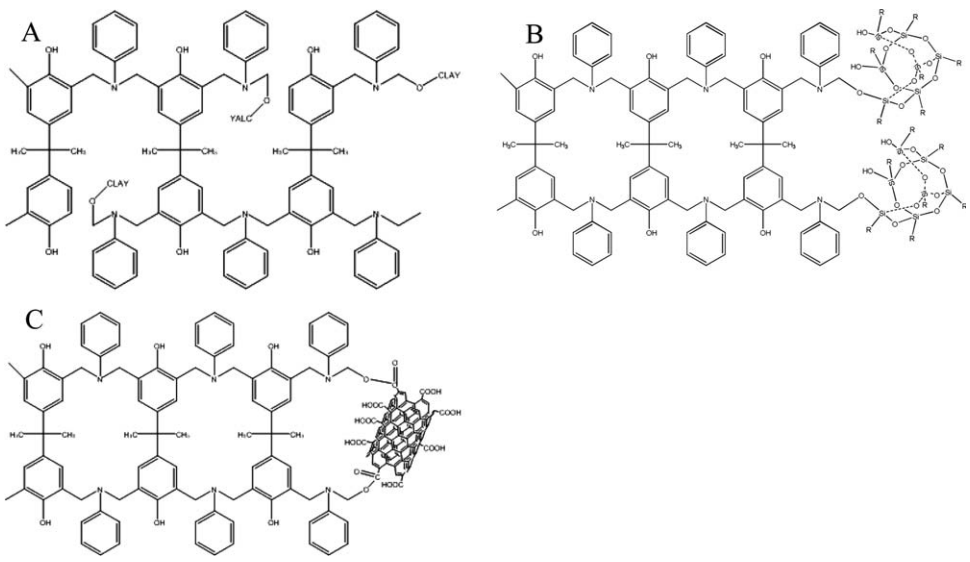

Figure 8. Scheme of crosslinked network formation of the (A) BEN/clay, (B) BEN/POSS, and (C) BEN/CNT nanocomposites.

the opening of the oxazine ring and the formation of benoxazine network are completed in a short period, rather than gradually or step by step formation of the network, which happened during the cure of cyanate ester. The self-dissociative reaction of oxazine ring occurred in initial stage, which produced free phenolic structures. These free phenolic groups further catalyze the ring opening reaction, resulting in the autocatalytic nature. Figure 7(C) shows the FTIR spectra for the BEN/30B clay resin cured at 180°C in nitrogen atmosphere (60 mL/min). The characteristic bands at 1076 and 998 cm^{-1} assigned to Si—O—Si asymmetric stretching and Si—O in-plane stretching respectively, indicated the presence of the 30 B clay. The procedure for monitoring the cure of the BEN/clay resin is the same as that of pure BEN resin. For the BEN/clay system, all the bands changed after 20 min, more quickly than that of the pure BEN system, which changed after 40 min. Thus, it is clear that the

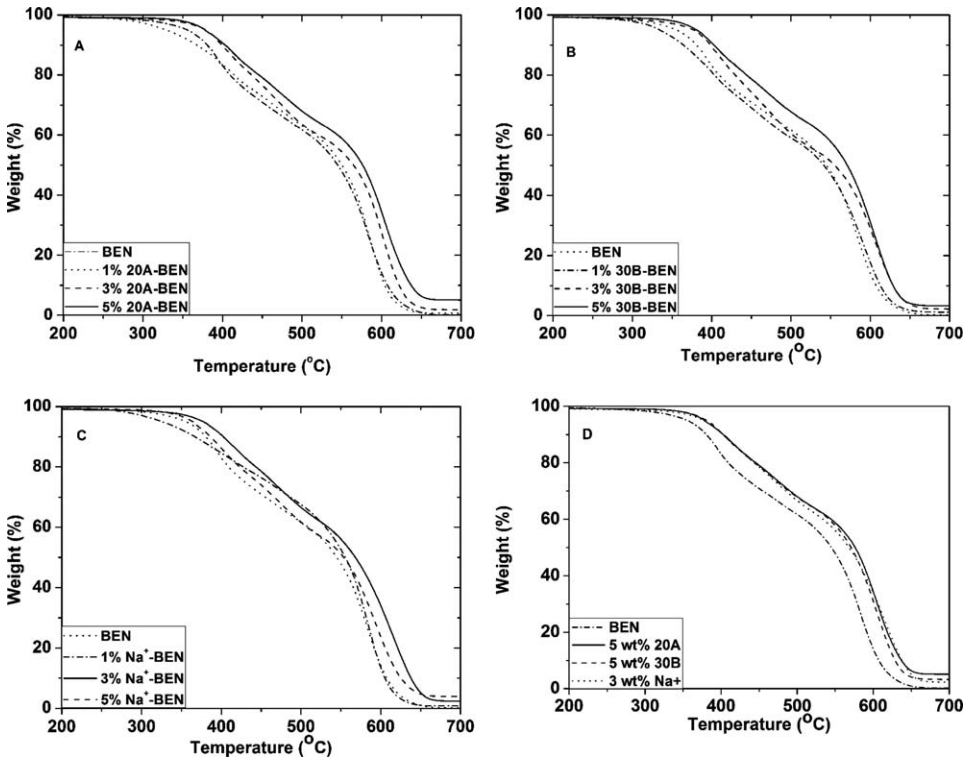

Figure 9. TG results of BEN/clay nanocomposites with residual weight in percentage versus temperature (A) 20A/BEN, (B)30B/BEN, (C) Na^+/BEN, and (D) comparative results for the clays performed best in each group.

Table V. Experimental Indicators for Thermal Stability from the TG Experiment

Sample	T_o	T_c	$T_{1/2}$	Char yield (wt %)
Pure BEN	320	660	544	0
1 wt % 20A/BEN	280	644	551	1
3 wt % 20A/BEN	351	660	564	2
5 wt % 20A/BEN	351	660	576	5
1 wt % 30B/BEN	288	657	540	1
3 wt % 30B/BEN	329	664	555	2
5 wt % 30B/BEN	353	664	570	3
1 wt % Na^+/BEN	277	647	554	1
3 wt % Na^+/BEN	345	676	568	2
5 wt % Na^+/BEN	345	663	554	4

T_o: onset temperature at which decomposition started.
T_c: completion temperature at which decomposition finished.
$T_{1/2}$: half-life decomposition temperature at which 50 wt % weight loss of the initial weight occurred.

Table VI. Experimental Indicators for Thermal Stability from the TG Experiment

Sample	T_o	$T_{1/2}$	Char yield at 800°C (wt %)
Pure BEN	257	493	36
1 wt % 20A/BEN	257	481	36
3 wt % 20A/BEN	283	640	39
5 wt % 20A/BEN	315	671	40
1 wt % 30B/BEN	282	489	38
3 wt % 30B/BEN	253	513	39
5 wt % 30B/BEN	328	729	45
1 wt % Na^+/BEN	275	512	40
3 wt % Na^+/BEN	282	538	43
5 wt % Na^+/BEN	289	639	42

incorporation of the clay accelerated the cure process of the BEN. Apart from the bands present in the FTIR spectra of the cure of BEN, a new broad band is observed at 1027 cm^{-1} assigned to stretching of the ether C—O—C group. This observation indicated the reaction of the clay with the BEN during the cure. The FTIR spectra of the cure of 5 wt % POSS/BEN nanocomposite with time are given in Figure 7(D). The procedure for monitoring the cure of the BEN/POSS nanocomposite is the same as that of pure BEN resin. There was no accelerating effect with the addition of the POSS. The POSS reacted with

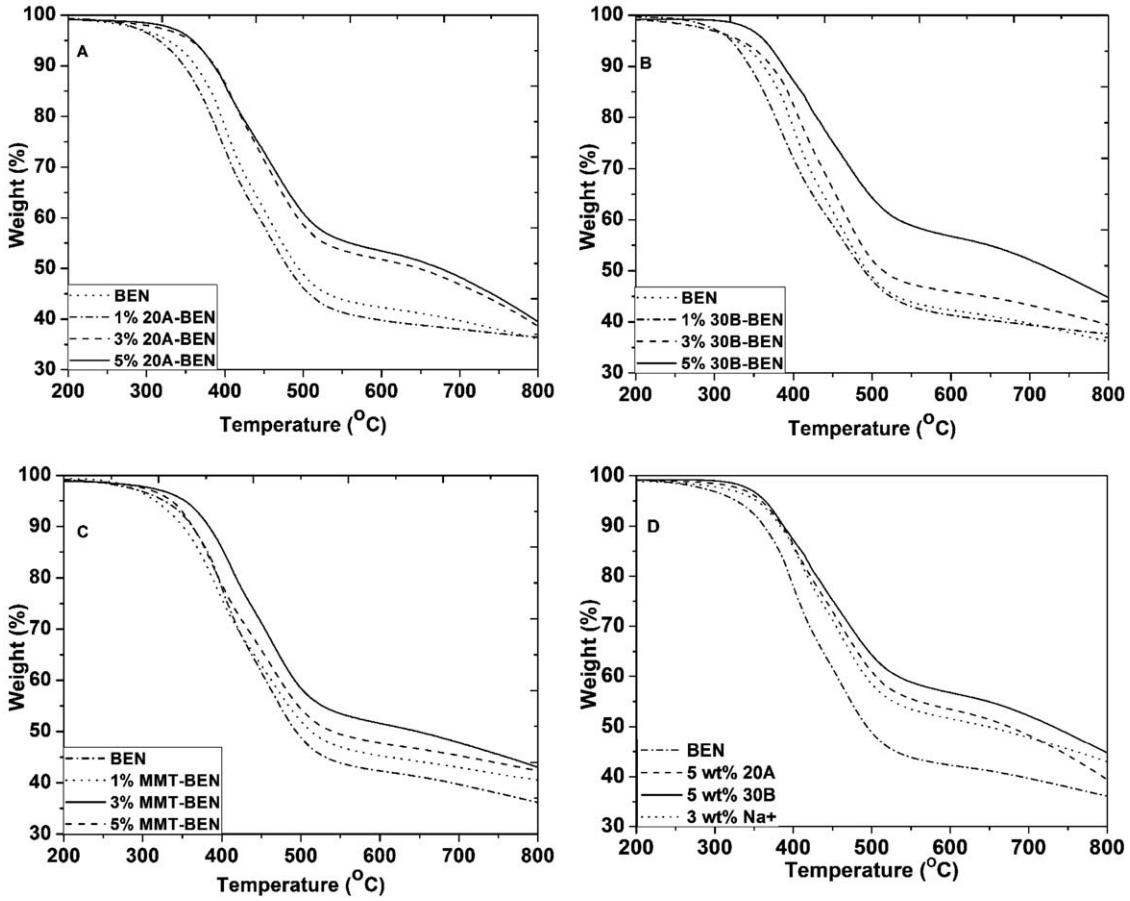

Figure 10. TG results of BEN/clay nanocomposites with residual weight in percentage versus temperature (A) 20A/BEN, (B)30B/BEN, (C) Na^+/BEN, and (D) comparative results for the clays performed best in each group.

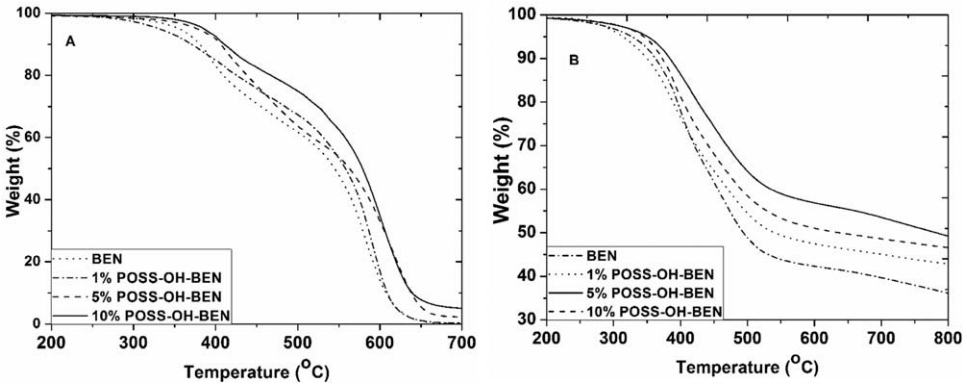

Figure 11. TG results of BEN/clay nanocomposites with residual weight in percentage versus temperature (A) under air atmosphere (20 mL/min), and (B) under nitrogen atmosphere (20 mL/min), with a heating rate of 10°C/min.

the BEN during the cure, proved by the presence of the band at 1050 cm^{-1}, indicating the formation of Si—O—C bond. Figure 7(E) shows the FTIR spectra for the BEN/MWCNT-COOH resin cured at 180°C in nitrogen atmosphere (60 mL/min). The characteristic band near 1650 cm^{-1} is assigned to C═O stretching, indicated the presence of the MWCNT-COOH. The procedure for monitoring the cure of the BEN/MWCNT-COOH resin is the same as that of pure BEN resin. For the BEN/MWCNT system, the addition of the CNT accelerated the cure process of the BEN. All the bands changed after 20 min, more quickly than for the pure BEN system, which changed after 40 min. Apart from the bands present in the FTIR spectra of the cure of BEN, two new bands are observed at 1250 and 1750 cm^{-1} assigned to stretching of the C—O bond and C═O bond, respectively. These two bands indicated the reaction of the MWCNT-COOH with the BEN to form an ester group. The scheme of the reaction of the nanofillers with BEN is shown in Figure 8.

Thermal Kinetics Analysis

The thermal stability of the pristine BEN, and its nanocomposites incorporating nanoclay, POSS, and CNT were evaluated by dynamic thermogravimertic analysis (TG). Figure 9 shows the TG results of the BEN/clay nanocomposites under air atmosphere. Table V lists the experimental indicators for thermal stability from the TG experiment. Under air atmosphere, the BEN became significantly less stable with the incorporation of 1 wt % of clays. Nevertheless, the incorporation of the clays with higher concentrations showed significant improvement to the thermal stability of BEN. For the 20A/BEN and 30B/BEN nanocomposites, the best performance was observed with the incorporation of the 5 wt % clays. For the Na^+/BEN nanocomposite, the best result showed when 3 wt % Na^+ was added. In Figure 9(D), the clays with best performance in each group were compared. There is not any obvious difference between them. The onset temperature increased from 320°C to about 350°C. The half life decomposition temperature also increased by 30°C. However, there is no improvement in full decomposition temperature with the incorporation of clays.

Figure 10 shows the TG results of the BEN/clay nanocomposites under nitrogen atmosphere. Table VI lists the experimental indicators for thermal stability from the TG experiment. Under nitrogen atmosphere, the BEN and its nanocomposites did not fully degrade even at temperatures in excess of 800°C. Generally, the incorporation of the clays with high concentration (over 1 wt %) showed significant improvement to the thermal stability of BEN. For the 20A/BEN nanocomposite and the 30B/BEN nanocomposite, the thermal stability increased with the increasing concentration. The best enhancement was observed with the incorporation of the 5 wt % clays. For the Na^+/BEN nanocomposite, the best result showed when 3 wt % Na^+ was added. As shown in Figure 10(D), the clays with best performance in each group were compared. The best enhancement for the thermal stability of the BEN was shown with the incorporation of 5 wt % 30B clay. The onset temperature was increased by 70°C. It is remarkable that the half-life decomposition temperature increased from 493 to 729°C, which is an improvement of 336°C. Furthermore, the char yield at 800°C increased 8 wt %.

Table VII. Experimental Indicators for Thermal Stability of BEN and its POSS Nanocomposite under Air Atmosphere

Sample	To	Tc	T1/2	Char yield (wt %)
Pure BEN	320	660	544	0
1 wt % POSS/BEN	264	668	558	0
5 wt % POSS/BEN	278	673	564	3
10 wt % POSS/BEN	338	684	578	5

Table VIII. Experimental Indicators for Thermal Stability of BEN and its POSS Nanocomposite under Nitrogen Atmosphere

Sample	T_o	$T_{1/2}$	Char yield at 800°C (wt %)
Pure BEN	257	493	36
1 wt % POSS/BEN	263	537	43
5 wt % POSS/BEN	278	773	49
10 wt % POSS/BEN	278	619	47

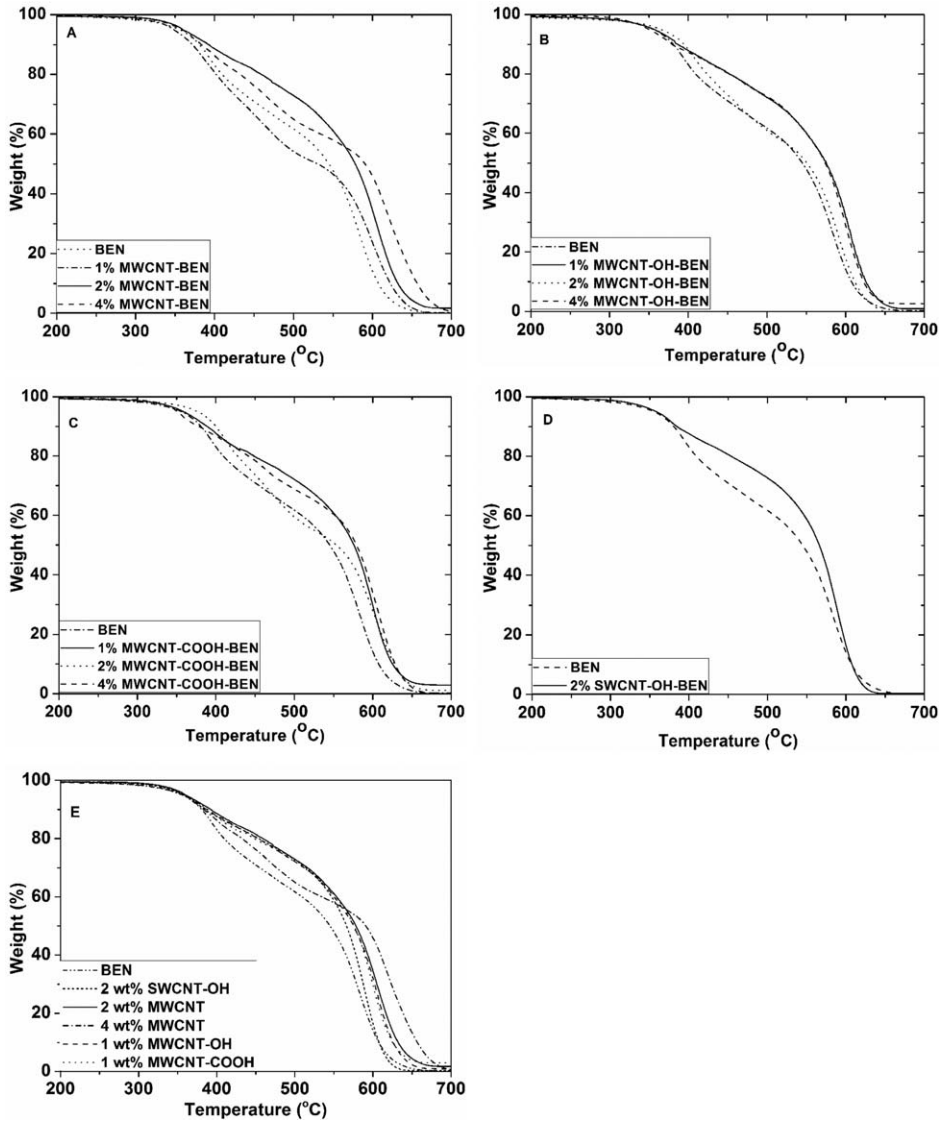

Figure 12. TG results of BEN/CNT with residual weight in percentage versus temperature (A) MWCNT/BEN, (B) MWCNT-OH/BEN, (C) MWCNT-COOH/BEN, (D) SWCNT-OH/BEN, and (E) comparative results, with a heating rate of 10°C/min under air atmosphere (20 mL/min).

Figure 11(A) shows the TG results of the BEN/POSS nanocomposite under air atmosphere. Table VII lists the experimental indicators for thermal stability from the TG experiment. Under air atmosphere, the incorporation of the POSS with high concentration showed good improvement to the thermal stability of the BEN. With the incorporation of 1 wt % POSS, the thermal stability of the BEN was slightly impaired at the temperatures lower than 400°C and the onset decomposition temperature reduced by 56°C. When the concentration is higher than 1 wt %, the thermal stability increased with increasing concentration. The best performance was observed with the incorporation of the 10 wt % POSS. The half-life decomposition temperature was increased by 34°C. Figure 11(B) shows the TG results of the BEN/clay nanocomposites under nitrogen atmosphere. Table VIII lists the experimental indicators for thermal stability from the TG experiment. Under nitrogen atmosphere, the BEN and its POSS nanocomposites did not fully degrade even if the temperature rose to 800°C. With the incorporation of 1 wt %

Table IX. Experimental Indicators for Thermal Stability from the TG Experiment

Sample	T_o	T_c	$T_{1/2}$	Char yield (wt %)
Pure BEN	320	660	544	0
1 wt % MWCNT/BEN	305	665	529	0
2 wt % MWCNT/BEN	319	675	577	2
4 wt % MWCNT/BEN	319	692	590	1
1 wt % MWCNT-OH/BEN	310	662	573	1
2 wt % MWCNT-OH/BEN	254	643	550	0
4 wt % MWCNT-OH/BEN	311	663	573	4
1 wt % MWCNT-COOH/BEN	317	662	575	3
2 wt % MWCNT-COOH/BEN	310	672	552	1
4 wt % MWCNT-COOH/BEN	316	662	579	0
2 wt % SWCNT-OH/BEN	313	640	565	1

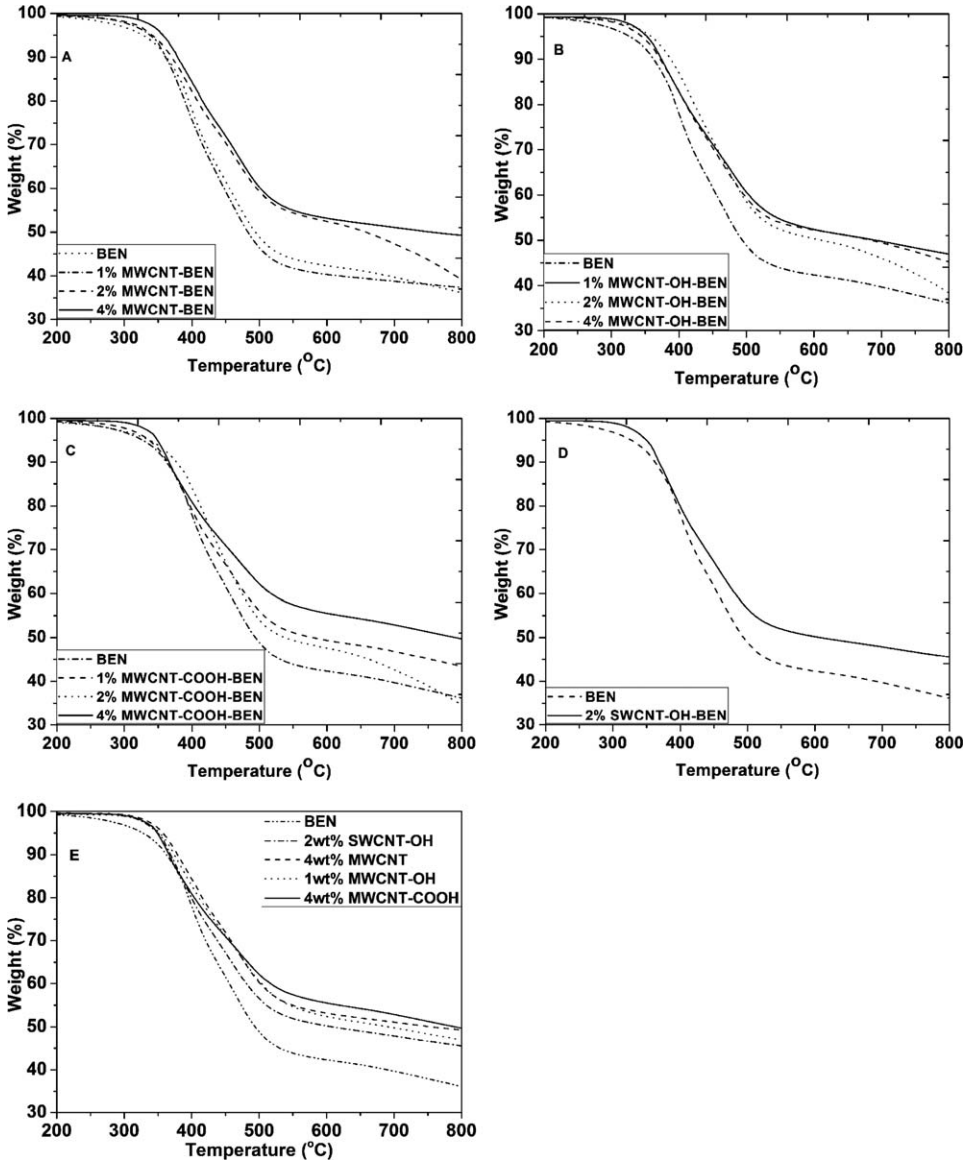

Figure 13. TG results of BEN/CNT nanocomposites with residual weight in percentage versus temperature (A) MWCNT/BEN, (B) MWCNT-OH/BEN, (C) MWCNT-COOH/BEN, (D) SWCNT-OH/BEN, and (E) comparative results under nitrogen atmosphere (20 mL/min).

POSS, the BEN was initially less thermally stable and became comparatively more stable with increasing temperature. The best performance was observed when 5 wt % POSS was incorporated. The half-life decomposition temperature and char yield were enhanced by 280°C and 13 wt %. The thermal stability of the 10 wt % BEN/POSS nanocomposite is better than that of pure BEN, but not as good as that of 5 wt % one.

Figure 12 shows the TG results of the BEN/CNT nanocomposite under air atmosphere. Table IX lists the experimental indicators for thermal stability from the TG experiment. In general, the addition of CNT improved the thermal stability of BEN, but the situation is very complex. For the MWCNT/BEN nanocomposites, the incorporation of 1 wt % MWCNT impaired the thermal stability. For the 2 and 4 wt % MWCNT/BEN nanocomposites, the thermal stability was enhanced, with the 2 wt % MWCNT/BEN nanocomposite performing better below 569°C. For the MWCNT-OH/BEN nanocomposites, the 1 and 4 wt % loaded nanocomposites showed similar enhancement to the thermal stability of BEN. For the MWCNT-COOH/BEN nanocomposites, the 2 wt % loaded nanocomposite was the most thermally stable below 412°C, with 1 wt % MWCNT-COOH/BEN nanocomposite performing best above 412°C. Furthermore, the thermal stability of 2 wt % SWCNT-OH/BEN nanocomposite is better than that of pure BEN. It can be seen from Figure 12(E) that 2 wt % MWCNT/BEN showed best thermal stability below 566°C, and 4 wt % MWCNT/BEN nanocomposite became most thermally stable above 566°C. With the incorporation of 4 wt % MWCNT, the half-life decomposition temperature was increased by around 40°C. In conclusion, the pure MWCNT displayed best performance among all of the CNTs.

Figure 13 shows the TG results of the BEN/CNT nanocomposite under nitrogen atmosphere. Figure 14 shows the TG results of

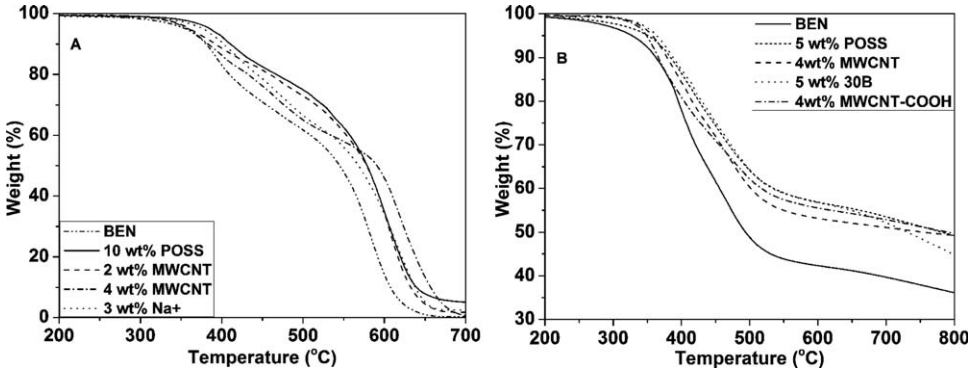

Figure 14. TG results of BEN based nanocomposites with residual weight in percentage versus temperature (A) under air atmosphere (20 mL/min), and (B) under nitrogen atmosphere (20 mL/min).

BEN/POSS and clayB30 nanocomposites under nitrogen and air atmospheres, respectively. Table X lists the experimental indicators for thermal stability from the TG experiment. In common with the analysis that under air atmosphere, the addition of CNTs improved the thermal stability of the BEN, but the situation is again very complex. For the MWCNT/BEN nanocomposites, the incorporation of 1 wt % MWCNT did not show much improvement to the thermal stability. The strongest reinforcement was observed with the incorporation of 4 wt % MWCNTs. For the MWCNT-OH/BEN nanocomposites, the 1 and 4 wt % loaded nanocomposites showed similar enhancement to the thermal stability of the BEN. MWCNT-OH/BEN (2 wt %) nanocomposite performed better below 464°C. For the MWCNT-COOH/BEN nanocomposites, the 2 wt % loaded nanocomposite was relatively thermally stable below 425°C, with 4 wt % MWCNT-COOH/BEN nanocomposite showing significantly enhancement above 412°C. Furthermore, the thermal stability of 2 wt % SWCNT-OH/BEN nanocomposite is better than that of the BEN. It can be shown from Figure 13(E) that 4 wt % MWCNT/BEN nanocomposite showed best thermal stability below 465°C, and 4 wt % MWCNT-COOH performed best above 465°C. With the addition of 4 wt % MWCNT, the onset decomposition of BEN increased by 74°C. For the 4 wt % MWCNT-COOH/BEN nanocomposite, the half-life decomposition temperature and char yield at 800°C increased by 286°C and 14 wt %, respectively. In conclusion, the type of CNT and concentration should be carefully chosen to fit typical application temperature range.

Table X. Experimental Indicators for Thermal Stability from the TG Experiment

Sample	T_o	$T_{1/2}$	Char yield at 800°C (wt %)
Pure BEN	257	493	36
1 wt % MWCNT/BEN	292	483	37
2 wt % MWCNT/BEN	304	654	39
4 wt % MWCNT/BEN	331	752	49
1 wt % MWCNT-OH/BEN	319	677	47
2 wt % MWCNT-OH/BEN	310	599	38
4 wt % MWCNT-OH/BEN	295	677	45
1 wt % MWCNT-COOH/BEN	285	575	44
2 wt % MWCNT-COOH/BEN	253	532	34
4 wt % MWCNT-COOH/BEN	323	779	50
2 wt % SWCNT-OH/BEN	318	594	46

Comparing with the TG curves of the various BEN based nanocomposites under air atmosphere, it can be seen that 10 wt % POSS /BEN showed the best thermal stability below 567°C, 4 wt % MWCNT/BEN nanocomposite became most thermally stable above 567°C. Interestingly, when comparing the TG curves of the BEN based nanocomposites under nitrogen atmosphere, 5 wt % POSS-OH/BEN performed the best thermal stability. Because of the different degradation mechanisms in different atmospheres, the concentration, the type of functional groups, and the type of fillers led to varied performance.

CONCLUSION

For the bisphenol-A benzoxazine (BEN), the incorporation of nanofillers rarely showed a catalytic effect, except for CNTs. The cure of the BEN based mixtures can be monitored by means of FTIR. The cure of the BEN followed a ring opening mechanism. All the functionalized nanofillers examined reacted with the BEN during the cure. However, the reaction between the nanofillers and the BEN did not lead to an acceleration of cure. The incorporation of the nanofillers showed good improvement to the thermal stability of both BEN. For the BEN, 10 wt % POSS /BEN showed the best thermal stability below 567°C, 4 wt % MWCNT/BEN nanocomposite became most thermally stable above 567°C, under air atmosphere Interestingly, 5 wt % POSS/ BEN exhibited the best thermal stability under nitrogen atmosphere.

REFERENCES

1. Ghosh, N. N.; Kiskan, B.; Yagci, Y. *Prog. Polym. Sci.* **2007**, *32*, 1344.
2. Ishida, H.; Agag, T. Handbook of Benzoxazine Resins; Amsterdam, Oxford: Elsevier, **2011**.
3. Nair, C. P. R. *Prog. Polym. Sci.* **2004**, *29*, 401.

4. Lee, Y. H.; Ishida, H. *Compos. Interface.* **2005**, *12*, 481.
5. Jang, J.; Seo, D. *J. Appl. Polym. Sci.* **1998**, *67*, 1.
6. Agag, T.; Takeichi, T. *High Perform Polym.* **2001**, *13*, S327.
7. Lee, Y. H.; Allen, D. J.; Ishida, H. *J. Appl. Polym. Sci.* **2006**, *100*, 2443.
8. Ishida, H.; Lee, Y. H. *J. Appl. Polym. Sci.* **2001**, *81*, 1021.
9. Ishida, H.; Lee, Y. H. *J. Polym. Sci.: Polym. Phys.* **2001**, *39*, 736.
10. Ishida, H.; Lee, Y. H. *Polymer* **2001**, *42*, 6971.
11. Takeichi, T.; Guo, Y.; Agag, T. *J. Polym. Sci.: Polym. Chem.* **2000**, *38*, 4165.
12. Cui, Y. J.; Chen, Y.; Wang, X. L.; Tian, G. H.; Tang, X. Z. *Polym. Int.* **2003**, *52*, 1246.
13. Ishida, H.; Allen, D. *J. Polymer* **1996**, *37*, 4487.
14. Espinosa, M. A.; Galia, M.; Cadiz, V. *Polymer* **2004**, *45*, 6103.
15. Rao, B. S.; Reddy, K. R.; Pathak, S. K.; Pasala, A. *Polym. Int.* **2005**, *54*, 1371.
16. Ishida, H.; Ohba, S. *J. Appl. Polym. Sci.* **2006**, *101*, 1670.
17. Zhu, C. L.; Wei, Y. Z.; Zhang, J.; Geng, P. F.; Lu, Z. J. *J. Appl. Polym. Sci.* **2014**, 131, 40960.
18. Sponton, M.; Estenoz, D.; Lligadas, G.; Ronda, J. C.; Galia, M.; Cadiz, V. *J. Appl. Polym. Sci.* **2012**, *126*, 1369.
19. Zhang, K.; Zhuang, Q. X.; Liu, X. Y.; Yang, G.; Cai, R. L.; Han, Z. W. *Macromolecules* **2013**, *46*, 2696.
20. Dumas, L.; Bonnaud, L.; Olivier, M.; Poorteman, M.; Dubois, P. *Eur. Polym. J.* **2014**, *58*, 218.
21. Huang, K. W.; Kuo, S. W. *Macromol. Chem. Phys.* **2010**, *211*, 2301.
22. Tseng, M. C.; Liu, Y. L. *Polymer* **2010**, *51*, 5567.
23. Du, W. J.; Shan, J. J.; Wu, Y. X.; Xu, R. W.; Yu, D. S. *Mater. Des.* **2010**, *31*, 2698.
24. Cui, H. W.; Kuo, S. W. *Polym Bull.* **2013**, *70*, 3143.
25. Yang, C. C.; Lin, Y. C.; Wang, P. I.; Liaw, D. J.; Kuo, S. W. *Polymer* **2014**, *55*, 2044.
26. Wang, C. F.; Kuo, S. W.; Lin, C. H.; Chen, H. G.; Liao, C. S.; Hung, P. R. *RSC Adv.* **2014**, *4*, 36012.
27. Dumas, L.; Bonnaud, L.; Olivier, M.; Poorteman, M.; Dubois, P. *Chem. Commun.* **2013**, *49*, 9543.
28. Chen, Q.; Xu, R. W.; Yu, D. S. *Polymer* **2006**, *47*, 7711.
29. Demir, K. D.; Tasdelen, M. A.; Uyar, T.; Kawaguchi, A. W.; Sudo, A.; Endo, T.; Yagci, Y. *J. Polym. Sci.: Polym. Chem.* **2011**, *49*, 4213.
30. Vengatesan, M. R.; Devaraju, S.; Dinakaran, K.; Alagar, M. *Polym. Compos.* **2011**, *32*, 1701.
31. Kuo, S. W.; Chang, F. C. *Prog. Polym. Sci.* **2011**, *36*, 1649.
32. Agag, T.; Takeichi, T. *Polym. Compos.* **2008**, *29*, 750.
33. Wang, Y. H.; Chang, C. M.; Liu, Y. L. *Polymer* **2012**, *53*, 106.
34. Alhassan, S. M.; Qutubuddin, S.; Schiraldi, D. A.; Agag, T.; Ishida, H. *Eur. Polym. J.* **2013**, *49*, 3825.
35. Lin, Y.; Song, M.; Stone, C. A.; Shaw, S. J. *Thermochim. Acta* **2012**, *552*, 77.
36. Kamal, M. R. *Polym. Eng Sci.* **1974**, *14*, 231.
37. Reading, M.; Hourston, D. J. Modulated Temperature Differential Scanning Calorimetry: Theoretical and Practical Applications in Polymer Characterisation. Hot Topics in Thermal Analysis and Calorimetry. Springer: Dordrecht, **2006**; Vol. *6*.
38. Lin, Y.; Stone, C. A.; Shaw, S. J.; Song, M. *J. Polym. Res.* **2013**, *20*, 1.
39. Stuart, B. H. Infrared Spectroscopy: Fundamentals and Applications; John Wiley & Sons, Ltd: Chichester, England, **2004**.